On the Effects of Intertidal Area on Estuarine Salt Intrusion

Hendrickx, Gijs G.; Pearson, Stuart G.

DOI
10.1029/2023JC020750

Publication date
2024

Document Version
Final published version

Published in
Journal of Geophysical Research: Oceans

JGR Oceans

RESEARCH ARTICLE

10.1029/2023JC020750

On the Effects of Intertidal Area on Estuarine Salt Intrusion

Gijs G. Hendrickx[1] and Stuart G. Pearson[1]

[1]Department of Hydraulic Engineering, Delft University of Technology, Delft, The Netherlands

Abstract Worldwide, estuaries are increasingly constrained by human interventions, such as wetland reclamations. Intertidal area has an important influence on the extent of estuarine salt intrusion. Previous research has shown conflicting effects of intertidal area on the salt intrusion. Therefore, this study explores this interaction for three estuary classes: (a) salt wedge, (b) partially mixed, and (c) well-mixed. Our findings show that the effect of intertidal area on the salt intrusion depends on the estuary class: enlarging the intertidal area reduces the salt intrusion for salt wedge and partially mixed estuaries, but vice versa for well-mixed estuaries. These opposing responses are explained by the balance between salt fluxes driven by the estuarine circulation versus by the tidal oscillation. In general, enlarging intertidal area results in the suppression of the estuarine circulation. Such system understanding is especially relevant in an era of increasing coastal urbanization.

Plain Language Summary Worldwide, estuaries are increasingly modified due to human activities, like reclaiming wetlands (i.e., areas that are submerged at high tide but exposed at low tide). Changes in these intertidal zones of estuaries can affect how far the salty water reaches inland, so-called salt intrusion. Past studies have given conflicting answers as to how the intertidal area influences salt intrusion. This study focuses on three classes of estuaries: (a) salt wedge (poorly-mixed), (b) partially mixed, and (c) well-mixed. We have found that the impact of the intertidal area on salt levels depends on the estuary class. Increasing the intertidal area reduces salt intrusion for salt wedge and partially mixed estuaries, while an opposite effect occurs in well-mixed estuaries. These different outcomes are connected to the balance between salt transport by density-driven currents and that driven by the tides. Our contribution to the understanding of these complex natural dynamics is of growing relevance in an age of magnified pressures on estuaries.

Key Points:

- Enlargement of the intertidal area can both increase and reduce estuarine salt intrusion
- The effect of the intertidal area on the estuarine salt intrusion depends on estuary class
- Enlargement of the intertidal area suppresses the estuarine circulation

Supporting Information:

Supporting Information may be found in the online version of this article.

Correspondence to:

G. G. Hendrickx,
G.G.Hendrickx@tudelft.nl

Citation:

Hendrickx, G. G., & Pearson, S. G. (2024). On the effects of intertidal area on estuarine salt intrusion. *Journal of Geophysical Research: Oceans*, *129*, e2023JC020750. https://doi.org/10.1029/2023JC020750

Received 24 NOV 2023
Accepted 17 JUN 2024

Author Contributions:

Conceptualization: Gijs G. Hendrickx, Stuart G. Pearson
Data curation: Gijs G. Hendrickx
Formal analysis: Gijs G. Hendrickx
Investigation: Gijs G. Hendrickx, Stuart G. Pearson
Visualization: Gijs G. Hendrickx
Writing – original draft: Gijs G. Hendrickx
Writing – review & editing: Gijs G. Hendrickx, Stuart G. Pearson

1. Introduction

Estuaries are human attractors due to their provision of freshwater and fertile soils, which has led them to become heavily modified over time (Pont et al., 2002). The supply of freshwater by the rivers is essential for these regions due to their connectivity with the sea, which promotes salinization—and thereby contamination—of the freshwater reserves (Costall et al., 2018). This can lead to water stress—that is, the shortage of freshwater (Wada et al., 2011)—, which is amplified by the high population densities found in coastal regions near estuaries. Water scarcity occurrences and their severity are likely to increase due to (relative) sea level rise, and increased frequency and duration of droughts induced by climate change (Distefano & Kelly, 2017; Veldkamp et al., 2015). In addition to their direct reduction of the freshwater supply, both sea level rise and increased droughts also promote salt intrusion, which indirectly puts a strain on the freshwater availability.

Meanwhile, estuaries are increasingly constrained due to human interventions, increasing their vulnerability to the changing environment (Pont et al., 2002). These human modifications often include the reduction of intertidal area and the channelization of the estuary: for example, the Westerschelde in the Netherlands (Nnafie et al., 2019; van Dijk et al., 2021); the Newark Bay in the United States (Chant et al., 2018); and the Yangtze River in China (Lyu & Zhu, 2019). These developments have increased the vulnerability of these estuarine systems to storm surges (e.g., Temmerman et al., 2013; Zhang et al., 2021) as well as salt intrusion, threatening the freshwater availability (e.g., Hendrickx et al., 2023; Yang & Wang, 2015). Besides the increased vulnerability, the channelisation and its associated reduction—or even complete removal—of intertidal area greatly damages the estuarine ecosystem (e.g., Seitz et al., 2014; van der Wal et al., 2017; van Wesenbeeck et al., 2014).

Recent studies have shown that intertidal areas influence the salt intrusion in estuaries (e.g., Geyer et al., 2020; Hendrickx et al., 2023; Lyu & Zhu, 2019; Siemes, 2024; Zhou et al., 2020), hence the freshwater availability. Tidal flats have been found to reduce salt intrusion (Hendrickx et al., 2023; Lyu & Zhu, 2019), but their influence

Table 1
Input Parameters Including Their Values or Ranges and Corresponding Units

Parameter	Symbol	Value	Unit
Tidal range	a	1.0–4.0	m
River discharge	Q	200–10,000	$m^3\ s^{-1}$
Channel depth	d_c	10.0	m
Channel width	W_c	2,500	m
Flat depth ratio	r_d	−1.0–1.0	–
Flat width ratio	r_W	1.0–2.0	–
Bottom friction	n	0.023	$m^{-1/3}s$
Convergence	γ	5.6×10^{-5}	m^{-1}

Note. The idealized geomorhology of the estuaries is inspired by the Westerschelde (The Netherlands), Pungue (Mozambique), and Hau (Vietnam).

has also been shown to be negligible, or even enhance salt intrusion (Siemes, 2024). This discrepancy begs the question of what the influence of intertidal areas is on salt intrusion, and what the underlying mechanisms are.

The aim of this paper is to investigate the effects of intertidal area on the salt intrusion for different estuary classes. Thereby we address the research question how tidal flats influence estuarine salt intrusion. Instead of exploring all possible estuarine configurations (as in, e.g., Hendrickx et al., 2023), we limit ourselves to the three main estuary classes allowing for a more detailed analysis.

2. Method

Central to this study on the effect of intertidal areas on the salt intrusion is a sensitivity analysis exploring different descriptions of tidal flats (Section 2.1). The effects are determined using a three-dimensional hydrodynamic model: Delft3D Flexible Mesh (Section 2.2); and we use a salt flux decomposition to distinguish the driving mechanisms of salt transport. This decomposition method is presented in Section 2.3.

2.1. Sensitivity Analysis

To explore the effects of intertidal area on the salt intrusion, we use idealized estuarine morphologies: funnel-shaped estuaries with a centralized channel. The morphology of the idealized estuaries are inspired by the Western Scheldt (the Netherlands), Pungue (Mozambique), and Hau (Vietnam). These are defined by estuary-scale parameters in a similar fashion as in Hendrickx et al. (2023). The forcing conditions (tidal range and river discharge) and the parametric design of the tidal flats are varied to investigate their effects on the salt intrusion in an estuary. Table 1 gives an overview of the input space explored in this study.

The depth and width of the tidal flats follow from two ratios we have varied (Table 1): (a) the flat depth ratio, r_d ($\in \{0.00, 0.25, \ldots, 1.00\}$); and (b) the flat width ratio, r_W ($\in \{1.0, 1.2, \ldots, 2.0\}$). These are similarly defined as in Hendrickx et al. (2023) resulting in the flat depth (d_f) and width (W_f):

$$d_f = \frac{1}{2} r_d a \tag{1}$$

where r_d is the flat depth ratio [–]; and a the tidal range [m];

$$W_f = (r_W - 1)\, W_c \tag{2}$$

where r_W is the flat width ratio [–]; and W_c the channel width [m].

Hendrickx et al. (2023) showed that spatially varying bottom friction—that is, separate bottom friction values for the channel and the intertidal areas—had little effect on the salt intrusion length. As such, we have applied a uniform bottom friction coefficient (n, Table 1).

The cross-sectional profile of the estuaries follow a generalized normal distribution. The flat depth ratio (r_d) defines the base of the distribution; and the flat width ratio (r_W) defines the cut-off of the distribution's tail (Figure 1a). Thus, the channel remains constant for all estuarine layouts to which an intertidal area is added based on these two ratios. These ratios are explored using a factorial space, which results in a two-dimensional space (r_d, r_W-space).

The effects of tidal flats on the salt intrusion are considered for three estuary classes: (a) salt wedge, (b) partially mixed, and (c) well-mixed. The classification is based on the estuarine Richardson number (Fischer, 1972):

$$Ri_E = \frac{g\beta s_0 Q}{W_c u_t^3} \tag{3}$$

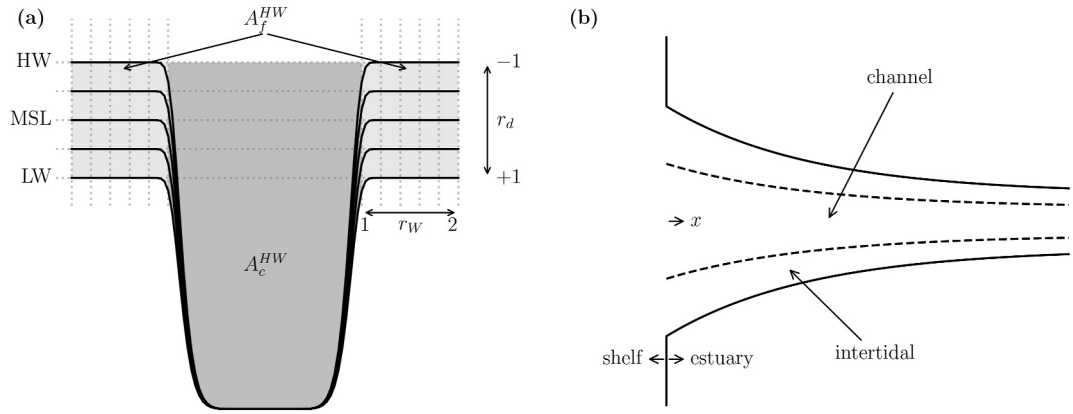

Figure 1. Parametric design of estuaries: (a) Cross-section: r_d is the flat depth ratio; r_W the flat width ratio (Table 1); A_c^{HW} the channel cross-sectional flow area; and A_f^{HW} the flat cross-sectional flow area (Equation 7). LW: low water; MSL: mean sea level; HW: high water. (b) Planar view.

where g is the gravitational acceleration [$g = 9.81$ ms^{-2}]; β the haline contraction coefficient [$\beta = 7.6 \times 10^{-4}$ psu^{-1}]; s_0 the salinity (at the mouth) [$s_0 = 30$ psu]; Q the river discharge [m^{3}s^{-1}]; W_c the channel width ($W_c = W - W_f = W/r_W$) [m]; and u_t the tidal flow velocity [ms^{-1}], which is estimated as:

$$u_t \approx \frac{a}{2\sqrt{2}}\sqrt{\frac{g}{d_c}}$$

where a is the tidal range [m]; and d_c the channel depth [m]. This estimation of the tidal velocity equals the root-mean-squared velocity of a monochromatic wave.

The estuarine Richardson number describes the level of stratification in the estuary resulting in the aforementioned three classes: (a) $Ri_E > 0.8$, salt wedge; (b) $0.08 < Ri_E < 0.8$, partially mixed; and (c) $Ri_E < 0.08$, well-mixed. The chosen forcing conditions—that is tidal range, a, and river discharge, Q—per class are given in Table 2 including their estuarine Richardson numbers. These forcing conditions result in similar classifications of the estuaries according to the classification by Geyer and MacCready (2014, not shown). Note that the forcing conditions representing the estuarine classes in Table 2 investigate only a small part of the input space to enable in-depth analyses of the driving mechanisms. For a fuller coverage of the input space, we refer the reader to Hendrickx et al. (2023).

2.2. Hydrodynamic Model

The idealized estuaries as described in Section 2.1 are simulated using a process-based hydrodynamic modeling software: Delft3D Flexible Mesh (Kernkamp et al., 2011). This software solves the Reynolds-averaged Navier-Stokes equations assuming hydrostatic pressure and implementing the k-ε turbulence closure model.

The model domain of the parametric design consists of two sub-domains: (a) the shelf, and (b) the estuary. The shelf domain is a square of 30 × 30 km. The grid resolution varies from 1,000 × 1,000 m at the offshore boundaries to 62.5 × 62.5 m near the mouth of the estuary. In between, the grid resolution transitions in steps of a factor of two: 500 × 500, 250 × 250, and 125 × 125 m. The different grid resolutions are connected using triangular grid cells.

The estuary domain is a deformed rectangle of 200 km length and varying width, depending on the intertidal area definition (Table 1). The deformation follows from the convergence, as the estuary's channel width exponentially decreases from 2,500 m (Table 1) to a minimum channel width of 600 m. The grid resolution in the estuary moves from 62.5 × 62.5 m at the mouth to <250 × 1,000 m at the upstream boundary. The high resolution region reached until 150 km landward after which the grid transitions to a coarser

Table 2
Boundary Conditions per Estuary Class

Class	a (m)	Q (m^{3}s^{-1})	Ri_E (–)
Salt wedge	1.0	10,000	16.2
Partially mixed	2.0	500	0.101
Well-mixed	4.0	200	0.00507

Note. The estuarine Richardson numbers are based on Equation 3.

resolution in a similar fashion as in the shelf domain. The <250 m near the upstream boundary follows from the deformation of the rectangular grid induced by the convergence.

Due to the focus on salt dynamics, the estuaries are simulated in three dimensions, where the vertical is discretisied with a hybrid Z, σ-layering. Five σ-layers are placed on top of the Z-layers, which are more suitable for computing pycnoclines (Stelling & van Kester, 1994). The interface between the two vertical discretization methods is at $z_{Z,\sigma} = -4.0$ m resulting in $\Delta\sigma \in [0.4, 1.2]$ m depending on the tidal range and moment in the tidal cycle. Within the estuarine domain, the Z-layers have equal thickness $\Delta Z = 1.0$ m, which grows beyond $z_{cst} = -10.0$ m in the offshore domain—that is, the shelf domain—with a factor of 1.10.

2.3. Salt Flux Decomposition

The transport of salt is driven by multiple factors with differing relevance depending on the boundary conditions and estuarine morphology. Decomposing the salt fluxes provides insights into these driving forces (e.g., Dronkers & van de Kreeke, 1986; Garcia et al., 2022; Lerczak et al., 2006; Ralston et al., 2010). The total salt flux is the product of the flow velocity and the salinity, integrated over the cross-sectional area normal to the flow velocity, positive in the landward direction:

$$F = \overline{\int us \, \mathrm{d}A} \tag{4}$$

where u is the flow velocity [ms^{-1}]; s the salinity [psu]; and A the cross-sectional area [m^2]. The over-bar represents temporal averaging over a tidal cycle.

The salt flux decomposition discriminates between four salt flux components: the salt flux related to (a) net flow or river discharge, (b) tidal oscillation, (c) estuarine circulation, and (d) time-dependent shear. These components are build up by differing the mathematical moment of temporal and/or spatial integration. Equations 5a–5e list the building blocks, where ξ is either representing the flow velocity, u, or the salinity, s:

$$\xi_1 = \frac{\overline{\int \xi \, \mathrm{d}A}}{\overline{\int \mathrm{d}A}} \tag{5a}$$

$$\xi_2 = \frac{\int \xi \, \mathrm{d}A}{\int \mathrm{d}A} - \xi_1 \tag{5b}$$

$$\xi_* = \xi - \xi_2 - \xi_1 \tag{5c}$$

$$\xi_3 = \frac{\overline{\xi_* \, \mathrm{d}A}}{\overline{\mathrm{d}A}} \tag{5d}$$

$$\xi_4 = \xi_* - \xi_3 \tag{5e}$$

Thus, ξ_1 represents the average over the tide and integration over the cross-section; ξ_2 the integration over the cross-section; ξ_3 the average over the tide; and ξ_4 the remainder. The sum of the flow velocity components, that is, Equations 5a–5e with $\xi = u$, equals the flow velocity, u: $\sum_{i=1}^{4} u_i = u$. Subsequently, the resulting four salt flux components are defined as:

$$F_1 = u_1 s_1 \overline{\int \mathrm{d}A} \tag{6a}$$

$$F_2 = \overline{u_2 s_2 \int \mathrm{d}A} \tag{6b}$$

$$F_3 = \int u_3 s_3 \, \mathrm{d}\overline{A} \tag{6c}$$

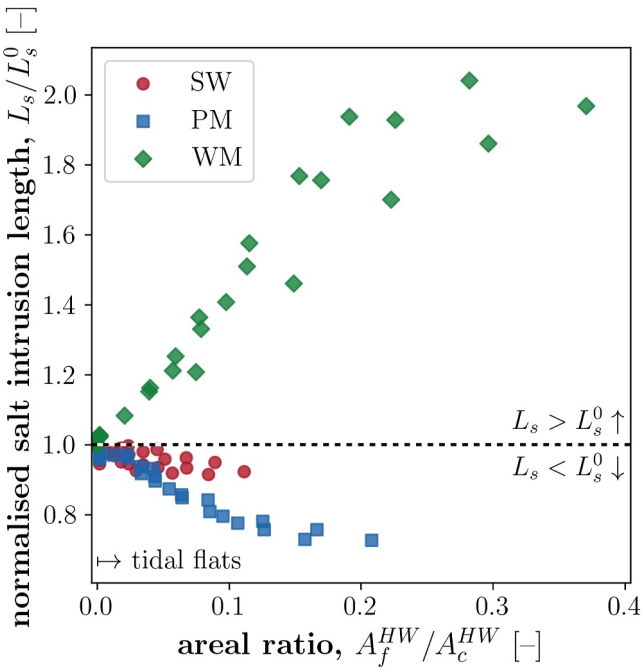

Figure 2. Influence of cross-sectional areas at high water on the salt intrusion length (Equation 7 and Figure 1a). SW: salt wedge; PM: partially mixed; WM: well-mixed.

$$F_4 = \overline{\int u_4 s_4 \, dA} \tag{6d}$$

where F_i follows the prior numbering of salt flux components [psu $m^3 s^{-1}$]: F_1 relates to the net flow; F_2 to the tidal oscillation; F_3 to the estuarine circulation; and F_4 to the time-dependent shear. The sum of these salt flux components represents the total salt flux:

$$F \approx \sum_{i=1}^{4} F_i$$

The salt flux related to the net flow (F_1) is offshore-directed (negative), compensating for the other components, which are generally all landward-directed (positive). The flux component related to the time-dependent shear is a residual term (Equation 5e) and generally an order of magnitude smaller than the other fluxes; therefore, it is often excluded from analyses or included in either F_2 or F_3 (e.g., Dronkers & van de Kreeke, 1986; Garcia et al., 2022; Lerczak et al., 2006; Ralston et al., 2010). In this study, we focus on the salt flux components related to the tidal oscillation (F_2) and the estuarine circulation (F_3) for these reasons.

3. Results

The salt intrusion length is normalized relative to the reference cases without tidal flats, L_s^0 (i.e., $r_W = 1.0$). The values of these reference salt intrusion lengths are $L_{s,SW}^0 = 11.9$ km (salt wedge), $L_{s,PM}^0 = 43.1$ km (partially mixed), and $L_{s,WM}^0 = 27.9$ km (well-mixed). The effects of the flat depth and width ratios (r_d and r_W) can be encapsulated by a single, combined variable: the wet cross-sectional area of the tidal flats. In Figure 2, the cross-sectional area of the channel as well as the tidal flats are considered at high water at the mouth of the estuary. This is reflected by adding the tidal amplitude to the depth profile:

$$A^{HW} = \int_W d(x_0, y) + \frac{1}{2}a \, dy \tag{7}$$

where $d(x_0, y)$ is the cross-section profile based on the generalized normal distribution at $x = x_0$, that is, at the mouth. The cross-sectional area of the channel, A_c^{HW}, considers the width-integration over the channel width (W_c); the remainder reflects the cross-sectional area of the tidal flats, A_f^{HW} (Figure 1a). Further results are presented using the areal ratio, A_f^{HW}/A_c^{HW} (similar to ratios used in Dronkers, 1978; Okubo, 1973).

The cross-sectional flow area of the tidal flats $\left(A_f^{HW}\right)$ increases from salt wedge to well-mixed estuaries (Figure 2) due to the larger tidal range imposed to achieve the different estuary classes (Table 2).

For both the salt wedge and partially mixed estuary classes, an increased areal ratio reduces the salt intrusion length, while the opposite is true for the well-mixed estuary (Figure 2). In case of the well-mixed estuary, increasing the intertidal area can more than double the salt intrusion length compared to the reference case (i.e., without intertidal area).

The spatial distributions of the salt flux components show a shift from being dominated by the estuarine circulation in a salt wedge estuary (Figure 3a) to tidal oscillation in a well-mixed estuary (Figure 3c). The introduction of intertidal area does little to change the dominant salt flux component in these estuaries that are strongly dominated by either the estuarine circulation or the tidal oscillation related salt fluxes.

However, the partially mixed estuary shows a transition between these salt flux components (Figure 3b), where the intertidal area has a profound influence on the spatial distribution of the salt flux components (Figure 4):

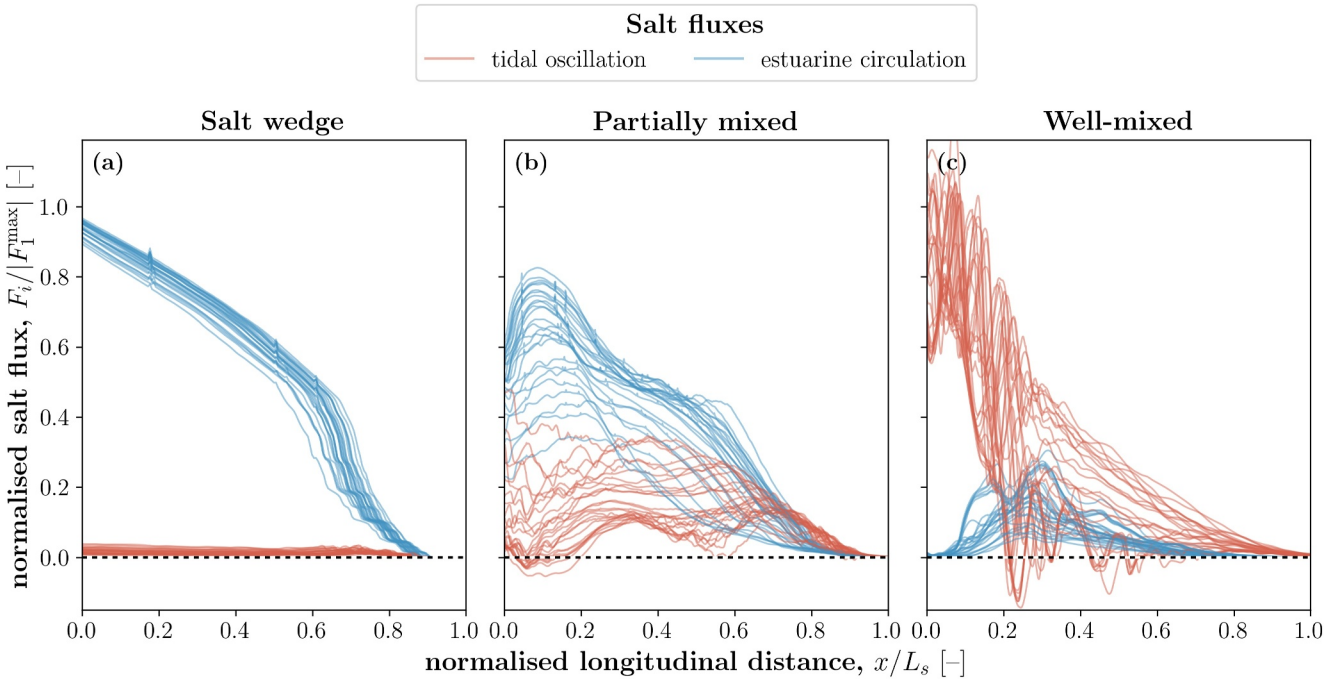

Figure 3. Spatial distribution of the major salt flux components (tidal oscillation and estuarine circulation) for all three estuary classes: (a) salt wedge, (b) partially mixed, and (c) well-mixed. The spatial distributions are displayed between the mouth (0.0) and the extent of the estuarine salt intrusion (1.0).

Increasing the intertidal area causes the dominant component of the landward salt flux to shift from estuarine circulation to tidal oscillation. A complete overview of all salt flux components and their dependencies on the areal ratio for all three estuary classes is given in Figure S1 in Supporting Information S1.

4. Discussion

Salt intrusion is affected by the expansion of intertidal area in two opposite directions: it increases for well-mixed estuaries; but decreases for salt wedge and partially mixed estuaries (Figure 2). In case of the well-mixed estuaries, the intertidal area facilitates the influx of saline water over the flats (Figure 5c). This influx is absent for the

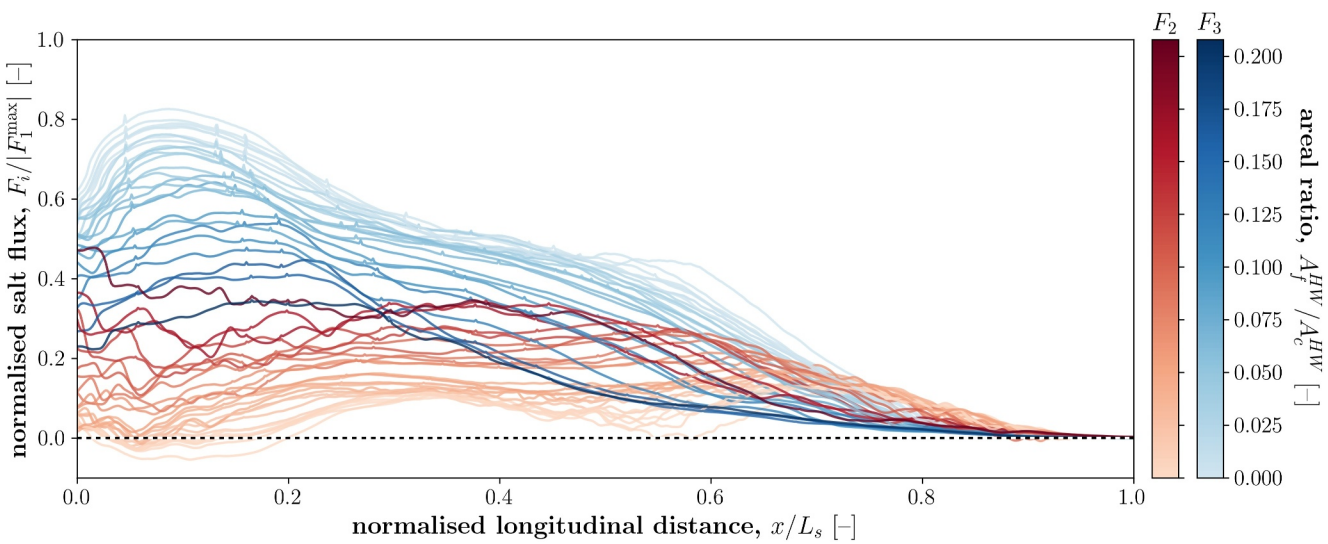

Figure 4. Spatial distribution of the major salt flux components: F_2, tidal oscillation (Equation 6b); and F_3, estuarine circulation (Equation 6c). The color-grading represents the areal ratio for the partially mixed estuary class (using Equation 2). Same data as Figure 3b.

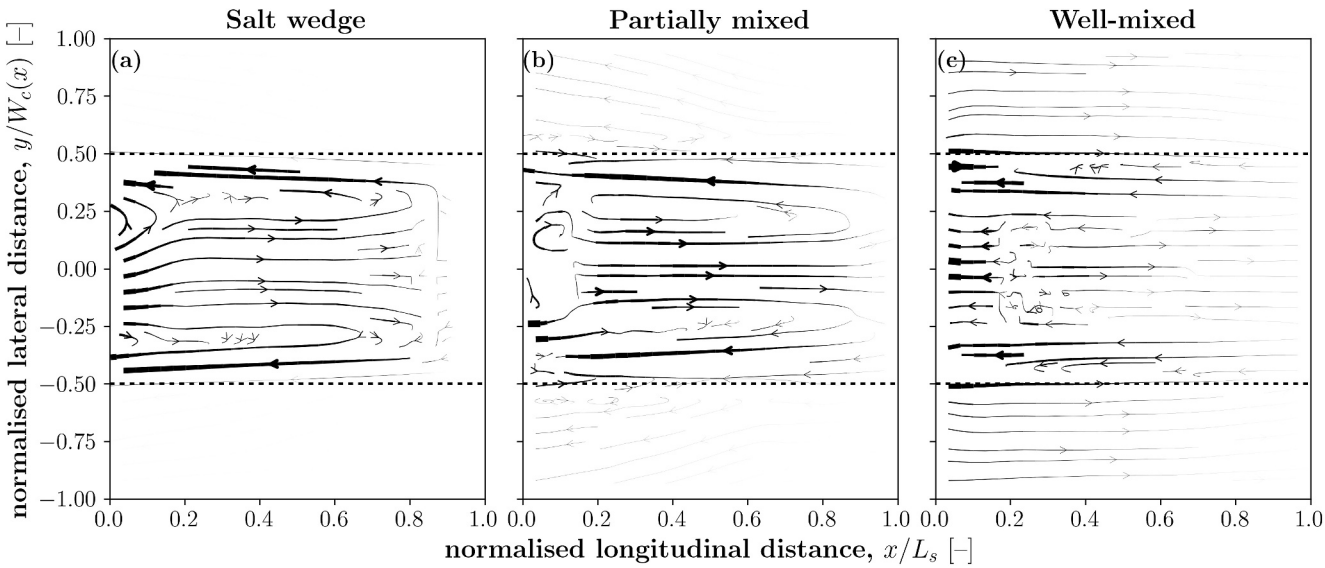

Figure 5. Streamlines of tide-averaged, depth-integrated salt fluxes (Equation 4) for the three estuarine classes: (a) salt wedge, (b) partially mixed, and (c) well-mixed. The flux-field represents the estuary with the maximum flat width (i.e., $r_W = 2.0$) and the flat depth at mean-sea-level (i.e., $r_d = 0.0$). The width of the streamlines represent the flux magnitude. Note that the y-axis is such normalized that the convergence of the estuary is compensated for.

other estuarine classes, where the salt fluxes are negligible on the intertidal areas (Figures 5a and 5b; in line with Geyer et al., 2020).

The influx over the intertidal flats in well-mixed estuaries increases with increasing intertidal area: Figure 6 distinguishes between the salt fluxes in the channel and on the tidal flats. For both the salt wedge and partially mixed estuaries, the in- and effluxes are balanced both in the channel and on the flats (Figures 6a and 6b); however, the flats are a strong importer of saline water for well-mixed estuaries, which is compensated for via the channel (Figure 6c).

In well-mixed estuaries, this influx over the intertidal area and efflux in the channel follows a typical barotropic circulation pattern (e.g., Bosboom & Stive, 2021; Kjerfve, 1978; Wang et al., 1999). This planar circulation pattern is also clearly visible in the residual flow patterns (Figure 7c). However, it is missing for the salt wedge

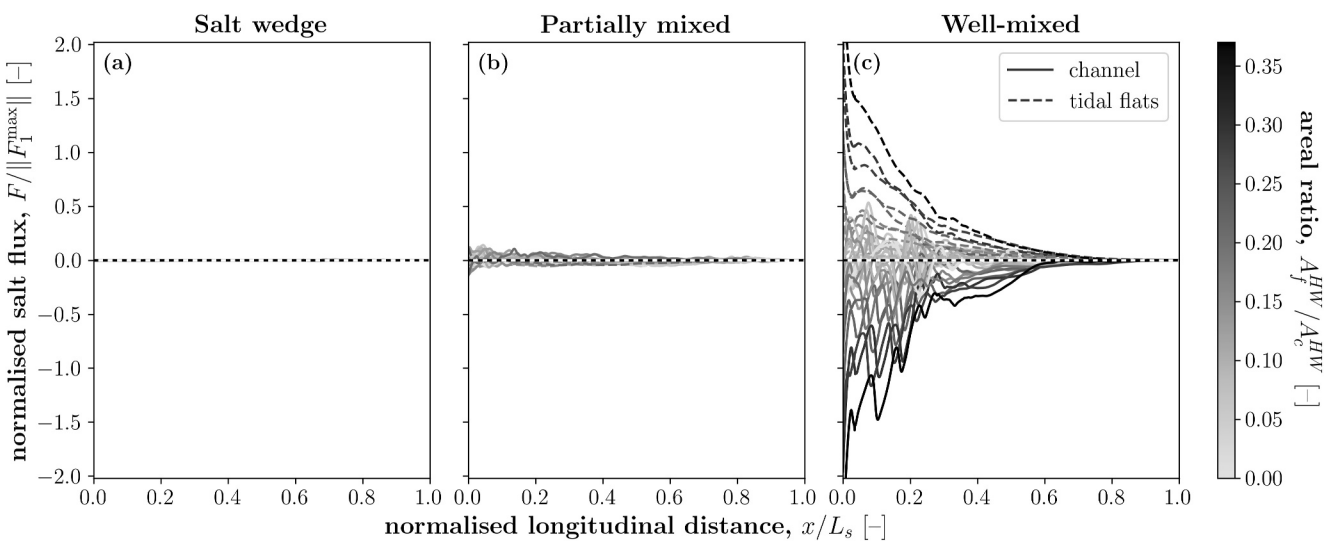

Figure 6. Spatial distribution of the total salt flux (Equation 4, F) distinguishing between the channel and the tidal flats for all three estuary classes: (a) salt wedge, (b) partially mixed, and (c) well-mixed.

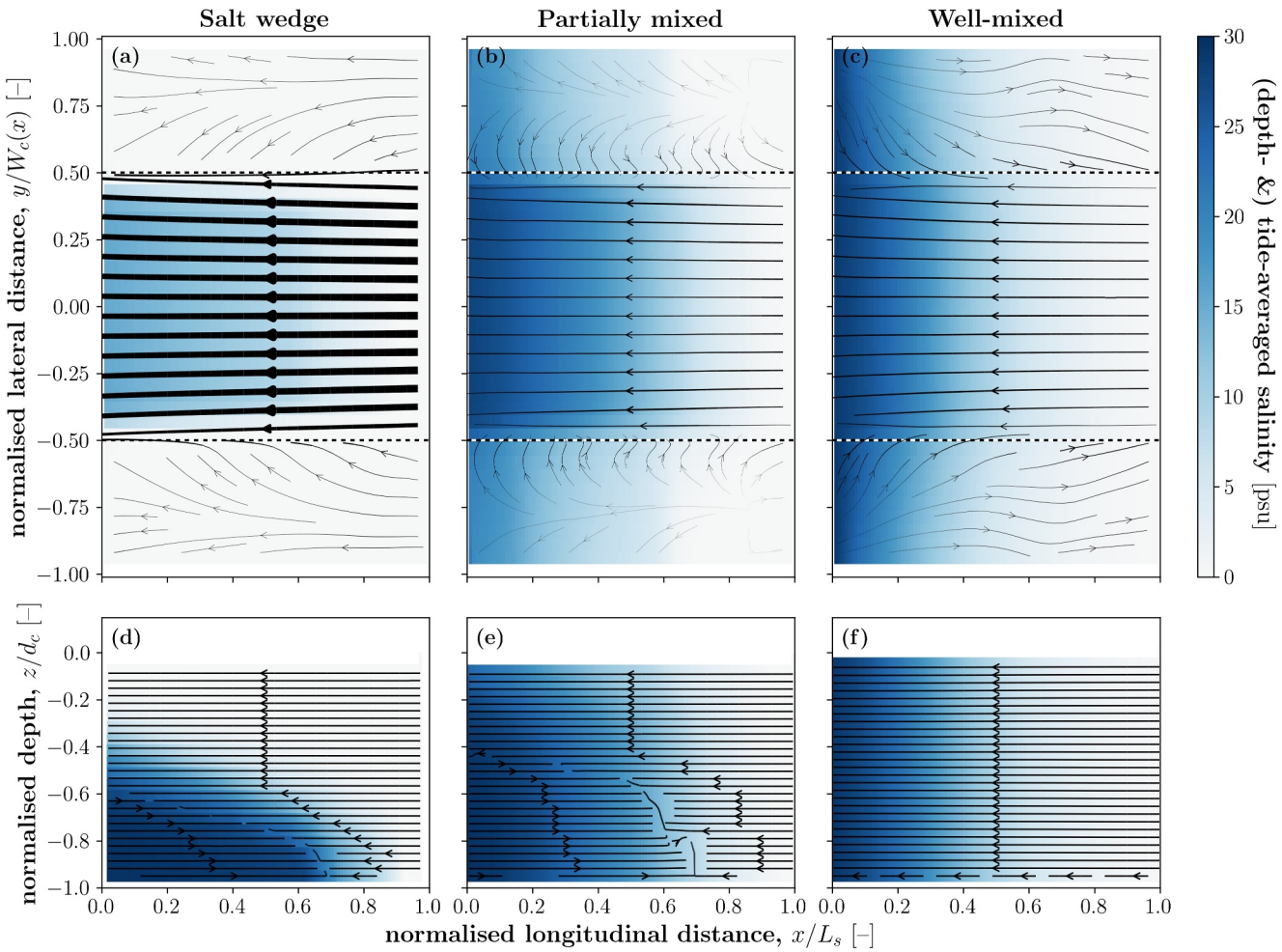

Figure 7. Spatial distribution of the flow velocity and salinity, both considered tide- (and depth-averaged), for all three estuary classes: (a, d) salt wedge, (b, e) partially mixed, and (c, f) well-mixed. The flow-fields are represented for the same estuaries as in Figure 5. The width of the streamlines represents the flow magnitude (in the top row); the blue-shading the salinity.

and partially mixed estuaries (Figures 7a and 7b). The negligible role of the intertidal area on the salt fluxes for the salt wedge estuary (Figure 6a) is in line with Geyer et al. (2020); and this statement can be extended to partially mixed estuaries as well (Figure 6b).

In addition to the total salt fluxes and flow patterns, the enhancement of intertidal areas also changes the distribution of salt flux components: Figure 4 shows an increasing dominance of the tidal oscillation of the landward salt flux with increasing intertidal area, that is, increasing areal ratio A_f^{HW}/A_c^{HW}. (An overview with all estuary classes is presented in Figure S1 in Supporting Information S1.)

In compound channels like those featured in this study, the abrupt depth change between shallow intertidal areas and the main channel enhances mixing (e.g., De Leo et al., 2022; Stocchino et al., 2011; van Prooijen et al., 2005). This mixing is intensified by the tidal influence (He et al., 2023). This increase in tidal mixing is reflected by an increased contribution of the tidal oscillation to the salt balance. To illustrate the relative contribution of the tidal flux, Hansen and Rattray (1965, 1966) proposed the use of a salt flux fraction. We have generalized this definition to reflect the importance of any of the salt flux components:

$$\nu_i = -\frac{F_i}{F_1} \tag{8}$$

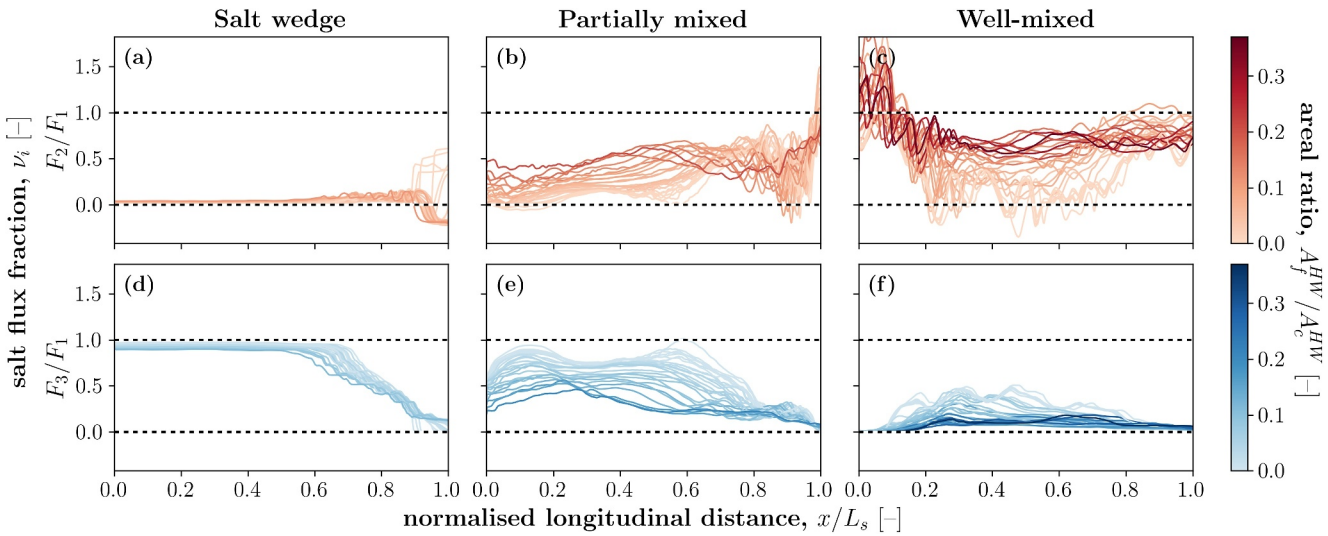

Figure 8. Salt flux fractions as function of the areal ratio related to (a–c) the tidal oscillation, ν_2; and (d–f) the estuarine circulation, ν_3, for all three estuary classes: (a, d) salt wedge, (b, e) partially mixed, and (c, f) well-mixed.

where F_i is salt flux i with $i \in \{2, 3\}$ (i.e., Equations 6b and 6c) [psu m^{3}s^{-1}]; and F_1 the salt flux related to the net flow (Equation 6a) [psu m^{3}s^{-1}].

As F_1 is the seaward-directed salt flux and the other salt flux components are landward directed, the flux fraction ν_i (Equation 8) quantifies the contribution—or fraction—of the salt flux F_i to the landward flux. Due to the opposing directions—that is, opposing signs—of the fluxes, Equation 8 includes a minus-sign such that $\nu_i \in [0, 1]$.

Estuarine circulation reduces with increasing intertidal area—as shown in Figure 4—for all three estuarine classes (Figures 8d–8f), whereas the tidal flux gains relevance (Figures 8a–8c). When the dominant salt flux component is related to the estuarine circulation, this suppression by the intertidal area reduces the salt intrusion; thus, suppressing the estuarine circulation in salt wedge and partially mixed estuaries decreases the salt intrusion (Figures 2a and 2b). However, in case the dominant salt flux is related to the tidal oscillation, reducing the estuarine circulation—and hence further enhancing the tidal flux—will promote salt intrusion; this is the case for well-mixed estuaries (Figure 2c). This is consistent with the increased tidal dispersion—and correspondingly salt intrusion—due to tidal trapping identified by Dronkers (1978) and Okubo (1973).

Note, however, that the fractions in Figure 8 do not always add up to 1—especially in case of the well-mixed estuary (Figures 8c and 8f). This discrepancy is related to a larger contribution of the time-dependent shear (F_4) for the partially mixed and well-mixed estuaries (Figure S1 in Supporting Information S1).

The suppression of the estuarine circulation by the introduction of intertidal area as found in this study contradicts the findings by Zhou et al. (2020). In their study, the addition of intertidal area instead stimulated the estuarine circulation. Their modeled increase in estuarine circulation was attributed to tidal straining (Zhou et al., 2020), using the decomposition method proposed by Burchard et al. (2011). Following this reasoning, the estuarine circulation must increase in our study as well, since our width-to-depth ratio favors tidal straining (Schulz et al., 2015). This discrepancy is expected to result from the inclusion of a net flow due to the river discharge in our study, which is neglected in the studies of Schulz et al. (2015) and Zhou et al. (2020). Furthermore, the simulations executed in our study consider the whole estuarine domain (Figure 1b), while Zhou et al. (2020) only consider a cross-sectional slice of the estuary. Thus, the baroclinic effects of enlarging the intertidal area are magnified where barotropic effects are dominant; for example, increasing ebb-dominance of an estuary generally reduces its salt intrusion (e.g., Cheng et al., 2013; Hendrickx et al., 2023; Pein et al., 2018).

In all of the estuaries we investigated, there is a shift from salt fluxes driven by estuarine circulation to tidal oscillation as the areal ratio increases (Figure 8). However, the effects of areal ratio on salt intrusion differ greatly (Figure 2): from mild reduction of the salt intrusion for salt wedge estuaries, substantial reduction of salt intrusion

Table 3
Simpson Number per Estuary Class Equation 9

Class	a (m)	Q (m^3s^{-1})	Ri_E (–)	Si (–)
Salt wedge	1.0	10,000	16.2	3.53
Partially mixed	*1.0*	*200*	*0.325*	*0.489*
	2.0	500	0.101	0.244
	4.0	*10,000*	*0.254*	*0.364*
Well-mixed	4.0	200	0.00507	0.0941

Note. Extended input space indicated in italics.

for partially mixed estuaries, to enhancement of salt intrusion in well-mixed estuaries. This discrepancy relates to the ability of the tidal mixing to overcome the stratification; a balance expressed by the Simpson number (e.g., Burchard et al., 2011; Geyer & MacCready, 2014; Simpson et al., 1990):

$$Si = -\frac{g\beta d_c^2}{c_f u_t^2}\frac{\partial s}{\partial x} \tag{9}$$

with

$$c_f = \frac{gn^2}{d_c^{1/3}}$$

where the longitudinal salinity gradient is determined on an estuary-scale, that is, based on the salt intrusion length; c_f is the nondimensional friction coefficient [–]; and n the Manning's n [$m^{-1/3}s$] (Table 1).

The partially mixed and salt wedge estuaries we investigated have a value $Si > 0.2$, which is marked as the transition value at which tidal mixing cannot overcome stratification throughout the tidal cycle (e.g., Cheng et al., 2013; Geyer & MacCready, 2014; Stacey & Ralston, 2005). The estuarine circulation scales with the Simpson number (Burchard & Hetland, 2010; Geyer & MacCready, 2014), and even more so for large Simpson numbers (i.e., $Si > 0.2$; Geyer & MacCready, 2014; Ralston et al., 2008). Thus, increasing the tidal mixing in such systems reduces the landward salt transport—that is, reduces the salt intrusion.

To further investigate this phenomenon, we extended the input space with two additional sets of boundary conditions representing estuaries classified as "partially mixed" (following Equation 3; see Table 3). Both added estuaries showed a similar response to the salt wedge estuary; that is, there is a weak reduction in the salt intrusion length for increasing intertidal area (not shown).

These scaling relations with the Simpson number and the findings of this study suggest the following: (a) for $Si > 0.2$ (permanently stratified), the addition of tidal mixing by enlarging the intertidal area reduces the salt intrusion length; (b) for $Si < 0.2$, the addition of tidal mixing enhances tidal dispersion causing the salt intrusion to increase; and (c) the mitigating effect of intertidal areas on salt intrusion increases the closer the Simpson number gets to its critical value, that is, $Si = 0.2$—so long as it remains above this value.

5. Conclusion

The enhancement or reduction of salt intrusion as a function of intertidal area depends on the estuary class (Figure 2): the enlargement of intertidal area reduces the salt intrusion in salt wedge and partially mixed estuaries; in well-mixed estuaries, the effect is opposite.

The driving mechanisms of salt intrusion—that is, the salt flux components (Equations 6a–6d)—are similarly affected by intertidal area, independent of estuary class. The estuarine circulation is damped by increasing intertidal area (Figure 8). As estuarine circulation is the dominant driver of landward salt transport in salt wedge and partially mixed estuaries, suppressing this mechanism results in a reduction of the salt intrusion. However, in well-mixed estuaries, the landward tidal salt flux is dominant, which is enhanced by enlarging the intertidal area. Therefore, the salt intrusion grows with increasing intertidal area in well-mixed estuaries.

Differences between our study and existing literature can be explained by several factors, including (a) the addition of a river discharge that influences both the longitudinal salinity gradient and the barotropic circulation patterns, which can dominate the system; and (b) the model design decisions, which may affect the connectivity between the channel and intertidal area (e.g., the type of vertical discretization).

Whether the enlargement of intertidal area increases or reduces salt intrusion has been linked to the Simpson-number (Si, Equation 9). For permanently stratified estuaries ($Si > 0.2$), the increase of intertidal area has a negative effect on the salt intrusion. This is because the introduced mixing due to the intertidal flats reduces the dominant salt flux driven by the estuarine circulation. On the other hand, for $Si < 0.2$, larger intertidal areas cause an increase in salt intrusion, as the additional mixing contributes to the tidal dispersion. The closer the Simpson

number is to its critical value of $Si = 0.2$ (i.e., the tipping point in the stratification-mixing balance), the stronger the influence of the intertidal area on the salt intrusion.

Data Availability Statement

The data set used in this study is publicly available (Hendrickx & Pearson, 2024) [Dataset] https://doi.org/10.4121/c357f1c7-dea8-4971-b5a1-c54c42e4172a.

Software availability: Processing code for the salt flux decomposition is open-source (Hendrickx, 2023) [Software]: https://doi.org/10.4121/bccbe767-667b-40ba-a4d1-d8fcad900772.

Acknowledgments
We are indebted to Peter M.J. Herman and Stefan G.J. Aarninkhof for their contributions to the early stages of the research design, which greatly added value to the study and subsequent manuscript. This work used the Dutch national e-infrastructure with the support of the SURF Cooperative using Grant EINF-4075. At last, we would also like to thank the two anonymous reviewers for their valuable feedback on the original manuscript; their suggestions greatly improved the manuscript. This publication is part of the project "Design and operation of nature-based SALTISolutions" (with project number P18-32 Project 7) of the research programme SALTISolutions which is (partly) financed by the Dutch Research Council (NWO).

References

Bosboom, J., & Stive, M. J. F. (2021). *Coastal dynamics*. TU Delft Open. https://doi.org/10.5074/T.2021.001

Burchard, H., & Hetland, R. D. (2010). Quantifying the contributions of tidal straining and gravitational circulation to residual circulation in periodically stratified tidal estuaries. *Journal of Physical Oceanography*, *40*(6), 1243–1262. https://doi.org/10.1175/2010JPO4270.1

Burchard, H., Hetland, R. D., Schulz, E., & Schuttelaars, H. M. (2011). Drivers of residual estuarine circulation in tidally energetic estuaries: Straight and irrotational channels with parabolic cross section. *Journal of Physical Oceanography*, *41*(3), 548–570. https://doi.org/10.1175/2010JPO4453.1

Chant, R. J., Sommerfield, C. K., & Talke, S. A. (2018). Impact of channel deepening on tidal and gravitational circulation in a highly engineered estuarine basin. *Estuaries and Coasts*, *41*(6), 1587–1600. https://doi.org/10.1007/s12237-018-0379-6

Cheng, P., de Swart, H. E., & Valle-Levinson, A. (2013). Role of asymmetric tidal mixing in the subtidal dynamics of narrow estuaries. *Journal of Geophysical Research: Oceans*, *118*(5), 2623–2639. https://doi.org/10.1002/jgrc.20189

Costall, A., Harris, B., & Pigois, J. P. (2018). Electrical resistivity imaging and the saline water interface in high-quality coastal aquifers. *Surveys in Geophysics*, *39*(4), 753–816. https://doi.org/10.1007/s10712-018-9468-0

De Leo, A., Tambroni, N., & Stocchino, A. (2022). Dispersion processes in weakly dissipative tidal channels. *Journal of Geophysical Research: Oceans*, *127*(10). https://doi.org/10.1029/2021JC018315

Distefano, T., & Kelly, S. (2017). Are we in deep water? Water scarcity and its limits to economic growth. *Ecological Economics*, *142*, 130–147. https://doi.org/10.1016/j.ecolecon.2017.06.019

Dronkers, J. (1978). Longitudinal dispersion in shallow well-mixed estuaries. In *Coastal Engineering 1978* (pp. 2761–2777). American Society of Civil Engineers. https://doi.org/10.1061/9780872621909.171

Dronkers, J., & van de Kreeke, J. (1986). Experimental determination of salt intrusion mechanisms in the Volkerak estuary. *Netherlands Journal of Sea Research*, *20*(1), 1–19. https://doi.org/10.1016/0077-7579(86)90056-6

Fischer, H. B. (1972). Mass transport mechanisms in partially stratified estuaries. *Journal of Fluid Mechanics*, *53*(4), 671–687. https://doi.org/10.1017/S0022112072000412

Garcia, A. M. P., Geyer, W. R., & Randall, N. (2022). Exchange flows in tributary creeks enhance dispersion by tidal trapping. *Estuaries and Coasts*, *45*(2), 363–381. https://doi.org/10.1007/s12237-021-00969-4

Geyer, W. R., & MacCready, P. (2014). The estuarine circulation. *Annual Review of Fluid Mechanics*, *46*(1), 175–197. https://doi.org/10.1146/annurev-fluid-010313-141302

Geyer, W. R., Ralston, D. K., & Chen, J. (2020). Mechanisms of exchange flow in an estuary with a narrow, deep channel and wide, shallow shoals. *Journal of Geophysical Research: Oceans*, *125*(12), e2020JC016092. https://doi.org/10.1029/2020JC016092

Hansen, D. V., & Rattray, M., Jr. (1965). Gravitational circulation in straits and estuaries. *Journal of Marine Research*, *23*, 104–122.

Hansen, D. V., & Rattray, M., Jr. (1966). New dimensions in estuary classification. *Limnology & Oceanography*, *11*(3), 319–326. https://doi.org/10.4319/lo.1966.11.3.0319

He, C., Yin, Z.-Y., Stocchino, A., & Wai, O. W. H. (2023). Generation of macro-vortices in estuarine compound channels. *Frontiers in Marine Science*, *10*(January), 1–15. https://doi.org/10.3389/fmars.2023.1082506

Hendrickx, G. G. (2023). NumPy-based salt flux decomposition. 4TU [Software]. *ResearchData*. https://doi.org/10.4121/bccbe767-667b-40ba-a4d1-d8fcad900772

Hendrickx, G. G., Kranenburg, W. M., Antolínez, J. A. A., Huismans, Y., Aarninkhof, S. G. J., & Herman, P. M. J. (2023). Sensitivity of salt intrusion to estuary-scale changes: A systematic modelling study towards nature-based mitigation measures. *Estuarine, Coastal and Shelf Science*, *295*, 108564. https://doi.org/10.1016/j.ecss.2023.108564

Hendrickx, G. G., & Pearson, S. G. (2024). Dataset underlying the study "On the effects of intertidal area on estuarine salt intrusion" [Dataset]. *4TU.ResearchData*. https://doi.org/10.4121/c357f1c7-dea8-4971-b5a1-c54c42e4172a

Kernkamp, H. W. J., Van Dam, A., Stelling, G. S., & de Goede, E. D. (2011). Efficient scheme for the shallow water equations on unstructured grids with application to the Continental Shelf. *Ocean Dynamics*, *61*(8), 1175–1188. https://doi.org/10.1007/s10236-011-0423-6

Kjerfve, B. (1978). Bathymetry as an indicator of net circulation in well mixed estuaries. *Limnology & Oceanography*, *23*(4), 816–821. https://doi.org/10.4319/lo.1978.23.4.0816

Lerczak, J. A., Geyer, W. R., & Chant, R. J. (2006). Mechanisms driving the time-dependent salt flux in a partially stratified estuary. *Journal of Physical Oceanography*, *36*(12), 2296–2311. https://doi.org/10.1175/JPO2959.1

Lyu, H., & Zhu, J. (2019). Impacts of tidal flat reclamation on saltwater intrusion and freshwater resources in the changjiang estuary. *Journal of Coastal Research*, *35*(2), 314–321. https://doi.org/10.2112/JCOASTRES-D-18-00077.1

Nnafie, A., de Swart, H. E., De Maerschalck, B., Van Oyen, T., van der Vegt, M., & van der Wegen, M. (2019). Closure of secondary basins causes channel deepening in estuaries with moderate to high friction. *Geophysical Research Letters*, *46*(22), 13209–13216. https://doi.org/10.1029/2019GL084444

Okubo, A. (1973). Effect of shoreline irregularities on streamwise dispersion in estuaries and other embayments. *Netherlands Journal of Sea Research*, *6*(1–2), 213–224. https://doi.org/10.1016/0077-7579(73)90014-8

Pein, J., Valle-Levinson, A., & Stanev, E. V. (2018). Secondary circulation asymmetry in a meandering, partially stratified estuary. *Journal of Geophysical Research: Oceans*, *123*(3), 1670–1683. https://doi.org/10.1002/2016JC012623

Pont, D., Day, J. W., Hensel, P., Franquet, E., Torre, F., Rioual, P., et al. (2002). Response scenarios for the deltaic plain of the Rhône in the face of an acceleration in the rate of sea-level rise with special attention to Salicornia-type environments. *Estuaries*, *25*(3), 337–358. https://doi.org/10.1007/BF02695978

Ralston, D. K., Geyer, W. R., & Lerczak, J. A. (2008). Subtidal salinity and velocity in the Hudson River estuary: Observations and modeling. *Journal of Physical Oceanography*, *38*(4), 753–770. https://doi.org/10.1175/2007JPO3808.1

Ralston, D. K., Geyer, W. R., & Lerczak, J. A. (2010). Structure, variability, and salt flux in a strongly forced salt wedge estuary. *Journal of Geophysical Research*, *115*(6), C06005. https://doi.org/10.1029/2009JC005806

Schulz, E., Schuttelaars, H. M., Gräwe, U., & Burchard, H. (2015). Impact of the depth-to-width ratio of periodically stratified tidal channels on the estuarine circulation. *Journal of Physical Oceanography*, *45*(8), 2048–2069. https://doi.org/10.1175/JPO-D-14-0084.1

Seitz, R. D., Wennhage, H., Bergström, U., Lipcius, R. N., & Ysebaert, T. (2014). Ecological value of coastal habitats for commercially and ecologically important species. *ICES Journal of Marine Science*, *71*(3), 648–665. https://doi.org/10.1093/icesjms/fst152

Siemes, R. W. A. (2024). *Modelling the effect of human interventions and climate change impacts on the sediment balance and salt intrusion in engineered estuaries*. (PhD Thesis). University of Twente. https://doi.org/10.3990/1.9789036562591

Simpson, J. H., Brown, J., Matthews, J., & Allen, G. (1990). Tidal straining, density currents, and stirring in the control of estuarine stratification. *Estuaries*, *13*(2), 125–132. https://doi.org/10.2307/1351581

Stacey, M. T., & Ralston, D. K. (2005). The scaling and structure of the estuarine bottom boundary layer. *Journal of Physical Oceanography*, *35*(1), 55–71. https://doi.org/10.1175/JPO-2672.1

Stelling, G. S., & van Kester, J. A. T. M. (1994). On the approximation of horizontal gradients in sigma co-ordinates for bathymetry with steep bottom slopes. *International Journal for Numerical Methods in Fluids*, *18*(10), 915–935. https://doi.org/10.1002/fld.1650181003

Stocchino, A., Besio, G., Angiolani, S., & Brocchini, M. (2011). Lagrangian mixing in straight compound channels. *Journal of Fluid Mechanics*, *675*, 168–198. https://doi.org/10.1017/S0022112011000127

Temmerman, S., Meire, P., Bouma, T. J., Herman, P. M. J., Ysebaert, T., & De Vriend, H. J. (2013). Ecosystem-based coastal defence in the face of global change. *Nature*, *504*(7478), 79–83. https://doi.org/10.1038/nature12859

van der Wal, D., Lambert, G. I., Ysebaert, T., Plancke, Y. M. G., & Herman, P. M. J. (2017). Hydrodynamic conditioning of diversity and functional traits in subtidal estuarine macrozoobenthic communities. *Estuarine, Coastal and Shelf Science*, *197*, 80–92. https://doi.org/10.1016/j.ecss.2017.08.012

van Dijk, W. M., Cox, J. R., Leuven, J. R., Cleveringa, J., Taal, M., Hiatt, M. R., et al. (2021). The vulnerability of tidal flats and multi-channel estuaries to dredging and disposal. *Anthropocene Coasts*, *4*(1), 36–60. https://doi.org/10.1139/anc-2020-0006

van Prooijen, B. C., Battjes, J. A., & Uijttewaal, W. S. J. (2005). Momentum exchange in straight uniform compound channel flow. *Journal of Hydraulic Engineering*, *131*(3), 175–183. https://doi.org/10.1061/(ASCE)0733-9429(2005)131:3(175)

van Wesenbeeck, B. K., Mulder, J. P., Marchand, M., Reed, D. J., de Vries, M. B., de Vriend, H. J., & Herman, P. M. (2014). Damming deltas: A practice of the past? Towards nature-based flood defenses. *Estuarine, Coastal and Shelf Science*, *140*, 1–6. https://doi.org/10.1016/j.ecss.2013.12.031

Veldkamp, T. I. E., Wada, Y., de Moel, H., Kummu, M., Eisner, S., Aerts, J. C. J. H., & Ward, P. J. (2015). Changing mechanism of global water scarcity events: Impacts of socioeconomic changes and inter-annual hydro-climatic variability. *Global Environmental Change*, *32*, 18–29. https://doi.org/10.1016/j.gloenvcha.2015.02.011

Wada, Y., van Beek, L. P. H., Viviroli, D., Dürr, H. H., Weingartner, R., & Bierkens, M. F. P. (2011). Global monthly water stress: 2. Water demand and severity of water stress. *Water Resources Research*, *47*(7). https://doi.org/10.1029/2010WR009792

Wang, Z. B., Jeuken, C., & de Vriend, H. J. (1999). *Tidal asymmetry and residual sediment transport in estuaries: A literature study and application to the Western Scheldt (Tech. Rep.)*. WL—Delft Hydraulics. Retrieved from http://repository.tudelft.nl/assets/uuid:08911ef5-5ee8-4a8b-9432-5a5a5dfaa142/z2749dr.pdf

Yang, Z., & Wang, T. (2015). Responses of estuarine circulation and salinity to the loss of intertidal flats: A modeling study. *Continental Shelf Research*, *111*, 159–173. https://doi.org/10.1016/j.csr.2015.08.011

Zhang, M., Dai, Z., Bouma, T. J., Bricker, J., Townend, I., Wen, J., et al. (2021). Tidal-flat reclamation aggravates potential risk from storm impacts. *Coastal Engineering*, *166*, 130868. https://doi.org/10.1016/j.coastaleng.2021.103868

Zhou, J., Stacey, M. T., Holleman, R. C., Nuss, E., & Senn, D. B. (2020). Numerical investigation of baroclinic channel-Shoal interaction in partially stratified estuaries. *Journal of Geophysical Research: Oceans*, *125*(4), e2020JC016135. https://doi.org/10.1029/2020JC016135